Cellulose (2024) 31:10341–10357
https://doi.org/10.1007/s10570-024-06154-7

ORIGINAL RESEARCH

Properties of quaternized and cross-linked hydroxyethylcellulose composite films

Ivan Šimkovic · Filip Gucmann · Edmund Dobročka · Jaroslav Filip · Michal Hricovíni · Viera Dujnič · Raniero Mendichi · Alberto Giacometti Schieroni · Daniele Piovani · Stefania Zappia · Miloš Hricovíni

Received: 12 June 2024 / Accepted: 30 August 2024 / Published online: 19 October 2024

Abstract Although trimetylammonium-2-hydroxypropyl-hydroxyethylcellulose (QHEC) is a well-known polysaccharide material, some of its properties have not been previously studied in detail. Therefore, we applied a combination of multidimensional nuclear magnetic resonance (NMR) in D_2O on hydroxyethylcellulose (HEC) and HEC derivatives, and size-exclusion chromatography with multi-angle laser light scattering (SEC-MALS) in carbonate buffer at pH 10; while Fourier-transform infrared spectroscopy (FTIR), the X-ray diffraction (XRD), the thermogravimetry/differential/differential thermogravimetry (TG/DTG/DTA) and atomic force microscopy (AFM) in film form. SEC-MALS revealed various water-solubility of prepared derivatives: HEC (98%) > CHEC (72%) > QHEC (26%) > QCHEC (14%). Due to its substituents, the HEC macromolecule forms coil structures with varying gyration radii: QHEC (38–260 nm) > QCHEC (10–230 nm) > CHEC (21–100 nm) > HEC (23–50 nm). FTIR analysis of all prepared films confirmed their identical structure compared to that observed in liquid form in D_2O. Onset temperatures (OT) of films degradation decreased in order: HEC (222 °C) > QCHEC (162 °C) > CHEC (142 °C) > QHEC (141 °C). The X-ray diffraction confirmed residual crystallinity of cellulose II (CII) in all four types of prepared films and was linked to ~ 2% water-insolubility of HEC derivatives revealed by SEC-MALS. Atomic force microscopy (AFM) showed significant differences in surface morphology among the four prepared films with surface roughness of: HEC (25 nm) > QCHEC (5.8 nm) > QHEC (4.2 nm) > CHEC (2.8 nm). Various spherical particles were found in case of HEC, circular depressions/holes approximately 4 µm in diameter were observed in case of QHEC. Except for the HEC, all other films showed granular surface probably due to insoluble components. Based on the mechanisms of quaternization and crosslinking and

Supplementary Information The online version contains supplementary material available at https://doi.org/10.1007/s10570-024-06154-7.

I. Šimkovic (✉) · M. Hricovíni · V. Dujnič · M. Hricovíni
Institute of Chemistry, Slovak Academy of Sciences, 845 38 Bratislava, Slovakia
e-mail: chemsimk@savba.sk

F. Gucmann · E. Dobročka
Institute of Electrical Engineering, Slovak Academy of Sciences, Dúbravská Cesta 9, 841 04 Bratislava, Slovakia

J. Filip
Department of Environmental Protection Engineering, Faculty of Technology, Tomas Bata University in Zlín, Zlín, Czechia

R. Mendichi
Expert Analysis, Molecular and Rheological Characterization Complex Polymers, Via Roma 7, 20067 Tribiano, Milan, Italy

A. G. Schieroni · D. Piovani · S. Zappia
Instituto di Scienze e Tecnologie Chimiche "G. Natta", Via A. Corti 12, 20133 Milan, Italy

the results of analysis on water-soluble part and films we could assume that there are similarities in structures between the soluble and insoluble products of the reactions.

Keywords 2-Hydroxyethylcellulose (HEC) · Quaternized 2-hydroxyethylcellulose (QHEC) · Cross-Linked 2-hydroxyethylcellulose (CHEC) · Quaternized and cross-linked hydroxyethylcellulose (QCHEC) · Film properties

Introduction

Polysaccharide composite materials are highly important ecologically-friendly alternative to synthetic polymers, due to their natural degradability after the end of their functionality (Solhi et al. 2023; Šimkovic 2008, 2013). The main reason causing this behaviour in polysaccharide composites is their ability to interact with water. Even though they are partially water-insoluble, they contain myriads of hydroxy groups, which cause water diffusion into these materials resulting in their swelling. Thanks to this, polysaccharide composites are easily exposed to various microorganisms allowing them to be degraded by enzymatic hydrolysis (Schaubeder et al. 2024; Diao et al. 2017). This phenomenon becomes more pronounced for materials with higher degree of water-solubility and leads to their faster degradation. Fibers resulting from pulping of wood are also partially water insoluble and negatively charged (Odabas et al. 2016). They might be reversed with quaternizing agent in water-miscible solvents to increase degree of substitution (DS). In this case the water-solubility/insolubility was monitored with FTIR, which supports cationization and C–N stretching vibration. In combination with NMR na SEC-MALS in water we could demonstrate that composition of water soluble and insoluble components is chemically identical and differs only in supramolecular structure. Recently also quaternization of cotton linters in tetraethyl ammonium hydroxide (TEAOH)/urea aqueous solution and NMR results demonstrated the substitution at C-2 and C-6 position (Xu and Cho 2024). Similarly important are also cellulose etherification reactions with glycidol, which result in 2,3-dihydroxypropyl cellulose or to crosslinking, depending uppon used conditions and solvent combination (Kim et al. 2024).

In the past, we have extensively studied the effect of crosslinking and quaternization in water on various polysaccharides, i.e., hyaluronic acid (Šimkovic et al. 2000), starch and polygalacturonic acid (Šimkovic et al. 2002), quaternized and sulfated xylan films (Šimkovic et al. 2014a), carboxymethylated- and hydroxypropylsulfonated xylan films (Šimkovic et al. 2014b), quaternized heparin films (Šimkovic et al. 2015), cross-linked and quaternized carboxymethyl cellulose (CMC) films (Šimkovic et al. 2021), as well as in extracts from agricultural by-products (Šimkovic et al. 2009a, b, 2010, 2017), and seaweed polysaccharide (Šimkovic et al. 2021). The polysaccharides containing ion-exchanging group have water-soluble fractions even when they are cross-linked. Some of the cross-linkers we have previously used, contained ion-exchanging group which improved the yields of the water-soluble fractions (Šimkovic and Jakab 2001).

2-Hydroxyethylcellulose (HEC) is a very important, water-soluble cellulose derivative, suitable for preparation of the multiple substituted polysaccharides (Del Giudice et al. 2017; Stoyneva et al. 2014). While in this study we prepared and studied bio-degradable HEC derivatives which can find purpose in various environmentally-friendly packaging technologies, HEC is widely used in many other applications such as a cement component to achieve its lower thermal conductivity (Cho et al. 2018). HEC films can also serve as a solid electrolyte when prepared with NH_4NO_3 (Li et al. 2014). Quaternized HEC is also important; it is used in textile industry for bonding of several types of dyes with ion-exchanging groups, and as a conditioner for hair and skin-care products (Busk et al. 2004). Various aspects of HEC films were studied in the past. Several studies reported their nanomechanical properties (Olson et al. 2021; Luo et al. 2023; Chu et al. 2019). Other studies used X-ray diffraction (XRD) to confirm the presence of HEC and reveal partial crystallinity related to cellulose II in the produced films (Diao et al. 2017; Langan et al. 2005). Quaternization of HEC to the primary hydroxy groups position was previously achieved also under the presence of nitrogen and isopropanol and characterized by elemental analysis and Fourier-transform infrared spectroscopy (FTIR) KBr technique (Wang and Ye 2010).

In the present work, our goal is to prepare quaternized (QHEC), cross-linked (CHEC), and quaternized

and cross-linked HEC (QCHEC) derivatives using one-step method and study their chemical and physical properties. Our results differed from those published previously on HEC derivatives (Yoshida et al. 2024), where those acted as liquid crystals with rod-like structures [(see proposed structures of HEC, QHEC, CHEC, and QCHEC in Supplementary Information (SI)]. Samples prepared in this study were extensively characterized by nuclear magnetic resonance (NMR) and size-exclusion chromatography with multi-angle light scattering (SEC-MALS) in solution. Film properties were evaluated by FTIR, XRD, atomic force microscopy (AFM) and thermal properties were studied by thermogravimetry (TG), derivative thermogravimetry (DTG), and differential thermal analysis (DTA). The prepared HEC derivatives showed good properties and even the QCHEC with lowest solubility (14%) yielded satisfactory results of the soluble part. We also confirmed by FTIR that samples in the form of films contained no structures other than those observed by NMR in the liquid form (D_2O). Our results are promising for further development of environmentally-friendly, biodegradable polysaccharide composite materials that can help to reduce the use of wide-spread synthetic plastics in some of the applications including packaging and protective coating, and therefore result in lower production of long-term stable waste, harmful for the environment and various organisms.

Experimental

Materials

2-Hydroxyethylcellulose (434,965-250G, Sigma-Aldrich; $M_w \sim 90{,}000$ g/mol; C, 44.00; H, 6.68). According to ^{1}H NMR integration of anomeric signals (see Fig. S2), the starting HEC contained 4.59% of 6-HEC, 20.95% of 2-HEC and 74.46% of unmodified cellulose. The degree of substitution (DS) was calculated with ^{1}H NMR integration of anomeric signals as: DS = Area of reaction anomeric signal/areas of all anomeric signals. For DS_{2HEC} = "4.57/1.00 + 4.57 + 16.24" = 0.21, while DS_{6HEC} = "1.00/1.00 + 4.57 + 16.24" = 0.05. Molecular substitution (MS) was calculated as: MS_{HEC} = Area of all anomeric substituents/Area of all anomeric signals = "1 + 4.57/16.24 + 1 + 4.57" = 0.26). Glycidyltrimethylammonium chloride (GTMAC, > 90%, 50,053-50ML, Sigma-Aldrich); sodium hydroxide (NaOH, SLAVUS), dialysis tubing [Union Carbide; 3.5 kDa molecular weight cut-off (MWCO)], epichlorohydrin (E, 99%, E-105–5, Sigma-Aldrich), and other chemicals were used without further purifications.

Quaternization of HEC

The HEC substrate [1.7324 g, 1 milli mole (mM); calculated assuming to the ^{1}H NMR integration (Fig. S8)] was mixed with 90 mL of water and NaOH (8 g; 0.2 mol) and stirred [1000 revolutions per minute (RPM); 2 h at room temperature], before GTMAC (7.45 mL; 0.05 mol) was added. After tempering at 60 °C/24 h/1000 RPM, the reaction was stopped by dilution with water. After that it was dialyzed (3.5 kDa MWCO) and lyophilized [1.8061 g of QHEC; 19.4% yield (actual weight of QHEC/theoretical weight of HEC + amount of GTMAC × 100 = 1.8061 g/1.7324 g + 7.5815 g of GTMAC); C, 46.00; H, 7.29; N, 0.78]. DS_Q = area of quaternization anomeric signal/area of all anomeric signals = "0.27/1.4 + 0.27 + 0.27" = 0.14; DS_{HEC} = "0.27/1.4 + 0.27 + 0.27" = 0.14 and MS_{Q+HEC} = "0.27 + 0.27/1.4 + 0.27 + 0.27" = 0.28.

Cross-linking of HEC

HEC (1.7324 g; 1 mM) was mixed with 90 mL of water and NaOH (8 g; 0.2 mol) and stirred (2 h/RT/1000 RPM), E (7.82 mL; 100 mM) was added and tempered (24 h/60 °C/1000 RPM) similarly to QHEC. The reaction was stopped by dilution with water and neutralized with HCl (from pH 12.6 to 8.85), dialyzed and lyophilized [1.8866 g of CHEC; 17.3% yield (1.8866 g of CHEC/1.8866 g of CHEC + 9.2 g of E); C, 46.08; H, 7.08 DS_C = Area of crosslinking anomeric signal/Area of unsubstituted cellulose anomeric signal + Area of HEC anomeric signal + Area of crosslinking anomeric signal = "0.04/2.52 + 1 + 0.04" = 0.01; DS_{HEC} = Area of HEC anomeric signal/Area of unsubstituted cellulose anomeric signal + Area of HEC anomeric signal + Area of crosslinking anomeric signal = "1/2.52 + 1 + 0.04" = 0.28 and MS_{C+HEC} = Area of crosslinking anomeric signal + Area of HEC anomeric signal/Area of unsubstituted anomeric

signal + Area of HEC anomeric signal + Area of crosslinking anomeric signal = "1.00 + 0.04/2.52 + 1.00 + 0.04" = 0.29.

Quaternization and cross-linking of HEC

HEC (1.7324 g; 1 mM) was mixed with 90 mL of water and NaOH (8 g; 0.2 mol), GTMAC (7.45 mL; 50 mM) and E (7.82 mL; 100 mM) were subsequently added and tempered (24 h/60 °C/1000 RPM) similarly to QHEC. The reaction was stopped by dilution with water, attonuating the pH to 10.3, dialyzed and lyophilized (2.3352 g of QCHEC; 12.6% yield (2.3352 g of QCHEC/1.7324 g of HEC + 7.5815 g of GTMAC + 9.2 g of E); (C, 46.78; H, 7.38; N, 0.72). DS_{QC} = Area of QC anomeric signal + Area of Q anomeric signal + Area of C anomeric signal/Area of unsubstituted anomeric signal + Area of Q anomeric signal + Area of C anomeric signal + Area of QC anomeric signal = "0.4/0.25 + 0.40 + 1.00" = 0.24; DS_{HEC} = 0.25/1 + 0.25 + 0.4 and MS_{QC+HEC} = Area of QC anomeric signal + Area of HEC anomeric signal + Area of Q anomeric signal + Area of C anomeric signal/Area of Unsubstituted anomeric signal + Area of HEC anomeric signal + Area of QC anomeric signal + Area of Q anomeric signal + Area of C anomeric signal = "0.4 + 0.24/1 + 0.25 + 0.4" = 0.39.

Films preparations

The films were prepared by mixing of 0.5 g of HEC and all the prepared derivatives, i.e., QHEC, CHEC, and QCHEC with 50 mL of deionized water (DW), then stirred at RT for 4 h at 1000 RPM and poured onto plastic petri dishes (5.5 cm in diameter). Resulting films were dried in the refrigerator at 5 °C until constant weight was achieved.

NMR analysis

All the studied samples were analyzed in D_2O, using Trimethylsilylpropionic acid (TSP) as internal standard; spectra of all used techniques are listed in SI section. In heteronuclear single quantum correlation spectroscopy combined with total correlation spectroscopy (HSQC-TOCSY) experiments, data mixing was 1024 × 256 (F2 × F1), and zero-filled to 2 K × 1 K giving the final resolution of 2.9 Hy × 23.5 Hy. 90 ms-long DIPSI-2 sequence was used for Hartmann-Hahn mixing. More details can be found elsewhere (Šimkovic et al. 2021, 2023).

Elemental analysis

The elemental compositions were analyzed using FLASH 2000 Organic elemental analyzer (Thermo Fisher Scientific; furnace temperature: 950 °C; PTFE column, 6 mm o. d. /5 mm i. d. × 2 m; 65 °C; helium was used as carrier and reference gas with respective flows of 140 and 100 mL/min; oxygen flow was 250 mL/min; run time was 720 s; 12 s sampling delay; 5 s injection end).

SEC-MALS analysis

The molecular weight distribution (MWD), size of macromolecules, the radius of gyration (R_g) w as obtained using an absolute multi-angle laser light scattering (MALS) detector connected to a size-exclusion chromatographic (SEC) system in water-carbonate buffer at pH 10. Rest of the conditions was identical as described previously (Šimkovic et al. 2021).

FTIR analysis

Fourier-transform infrared spectra were measured with spectrometer iS50 (Thermo Fisher Scientific, USA) equipped with DTGS detector and Omnic 9.0 software. The spectra were collected in the middle region from 4,000 to 400 cm^{-1} at a resolution of 4 cm^{-1}, the number of scans was 128. Diamond ATR was applied for measurement in solid/liquid state.

Thermal analysis

The experiments were run on NETCH STA 449F3 STAF3A-0382 instrument in air environment [50 mL/min and nitrogen balance maintenance (PG = 20 mL/min)]. 30 mg cut-outs from the prepared films were analyzed. The heating rate was 10 K/min and a Al_2O_3 pan was used. The onset temperatures (OT) were determined in parallel from DTA and DTG as a start

of exothermal and DTG start peaks after evaporation of physically-bound water.

XRD analysis

Similar to our previous work (Šimkovic et al. 2021), the XRD measurements were performed using Bruker D8 DISCOVER diffractometer equipped with X-ray source with rotating Cu anode with lamp operating at 12 kW power, 40 kV voltage, and 300 mA current. Parallel beam geometry with parabolic Goebel mirror in the primary beam was used; beam divergence was ~ 0.03°. To suppress the influence of surface roughness and other irregularities, and to avoid the change of size, shape, and X-ray penetration depth into the sample during the measurement, grazing incidence (GI) setup with constant angle of incidence $\alpha = 2°$ was used. Measurement was done in angular range 5°–40° with 0.05° step size, and 1 s integration time per step.

Cyclic voltammetry

Aqueous solutions of HEC, CHEC, QHEC, and QCHEC were prepared by dissolving the solid polymers in DW (10 mg mL^{-1}) and drop-casted on the surface of screen-printed carbon electrodes (SPE) with carbon counter and AgCl pseudo-reference electrode (DropSens, Spain). 5 µL of each solution were pipetted on the individual SPEs, and dried at RT in nitrogen atmosphere. After drying, deposition/drying steps were repeated twice to achieve thicker film on SPEs. Finally, prepared electrodes were connected via SPE connector (DropSens, Spain) to EmStat4S potentiostat (PalmSens, Netherlands). For measurements, 100 mL of 5 mM ferricyanide in 100 mM KCl was pipetted on the modified electrode surface and cyclic voltammetry was subsequently measured. The results are listed in SI.

AFM analysis

AFM-resolved surface morphology scans of all prepared films were recorded under ambient atmosphere using Ntegra Prima microscope (NT-MDT) in tapping mode. All scans were recorded in resolution of 512 × 512 px. Used probes were commercially available tips with nominal radius of curvature < 8 nm (HQ:NSC35/Al BS, Micromasch, https://www.spmtips.com/afm-tip-hq-nsc35-al-bs). ~ 1 × 1 cm^2 film cut-outs glued onto Si substrates were used as the samples for AFM measurement. Measured scans were processed in Gwyddion software (Nečas et al. 2012).

Results and discussion

Chemical modification

Using identical concentration of NaOH for the quaternization of HEC with GTMAC and cross-linking with E resulted in 19.4% and 17.3% yields, respectively. Both alkylating agents reacted preferentially with hydroxyethyl groups than with unmodified cellulose due to their better space availability (see Fig. S1 in SI). The slightly higher yield of quaternization could be explained by the formation of hydroxy groups at C–2 of GTMAC, which might be attacked with another molecule of E or GTMAC. The presence of HO^- anions by dissociation of NaOH in water cause an activation of hydroxyethyl groups and also a destruction of the epoxy ring of GTMAC and E. This resulted in low yields due to degradation of the alkylating agents into inactive by-product [$HO–CH_2–CH(OH)–CH_2–N^+(CH_3)_3$ (Xu and Cho 2024) and $HO–CH_2–CH(OH)–CH_2–OH$ (Cofer 1958)] as shown in Fig. 1.

As opposed to the unmodified cellulose hydroxy groups, the hydroxyethyl OH groups are cross-linked to multiple sites due to easier spatial availability and residual crystallinity of the unmodified cellulose (Gökmen and Bayramgil 2022). The combined modification of HEC by quaternization and cross-linking in one step gave the lowest yield (12.6%). Slightly smaller yield in case of QCHEC might be caused by slightly bigger spatial requirements for multiple hydroxyethyl groups to interact with negatively activated NaOH hydroxy groups during their reaction with quaternary groups. In comparison to published data, comparable results on nitrogen content (0.78% for QHEC or 0.72% for QCHEC) were obtained at more diluted conditions, absence of isopropanol, and using nitrogen atmosphere (Wang and Ye 2010). Their obtained nitrogen content was 0.79% at 10% dose of GTMAC; highest nitrogen content (1.16%) was achieved at 20% dose of GTMAC. According to

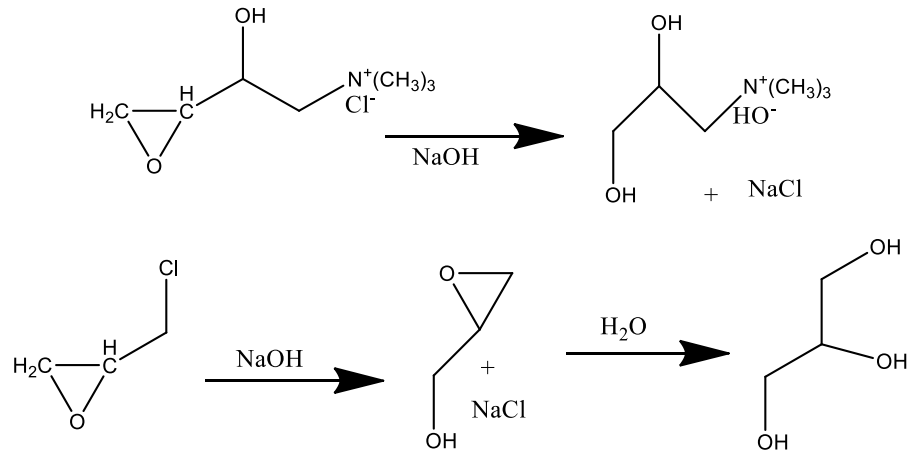

Fig. 1 Hydrolysis of GTMAC and E with NaOH

Wang and Ye, the modification took place primarily at the C_6 position. According to Zhou et al. (2005), the reactivity of the hydroxy groups decreased in order: Cellulose–O–CH_2–CH_2–OH > C_6 > C_2 > C_3, however these were established using less convincing one-dimensional ^{13}C NMR analysis with minimal chemical shift differences in NaOH/urea/D_2O (6/4/90) compared to our results (Zhou et al. 2005). Quaternization of wood delignified fibers confirmed better efficiency of quaternization in combination of mixable water-organic solvents (Odabas et al. 2016). Quaternization of cotton linters in tetraethylammonium hydroxide/urea aqueous solution, followed by acetic acid resulted in formation of cotton linters well-dissolved, leading to homogeneous quaternization (Xu and Cho 2024).

If the HEC hydroxy groups of Cellulose–O–CH_2–CH_2–OH could be alkalyzed with NaOH in water, when the formed nucleophyle (Cellulose–O–CH_2–CH_2–O^-) could attack the epoxy ring of GTMAC or E and form ether bond. In the case of GTMAC a new hydroxyl is formed on C_2 of the alkylating agent, which could undergo further alkylation by another molecule of GTMAC. The cross-linking mechanism through the 2-hydroxypropyl(trimethylammonium) group is analogous to (Zhou et al. 2005). The described mechanism (Fig. 2) is identical to that of the cross-linking of starch with E (Kuniak and Marchessault 1972).

NMR analysis

Three anomeric signals were observed in ^1H NMR spectrum (Fig. S2), of HEC [see hypothetical structure in Fig. S1 in Supplementary information (SI)] when integrated at 15 °C: at 4.54 ppm

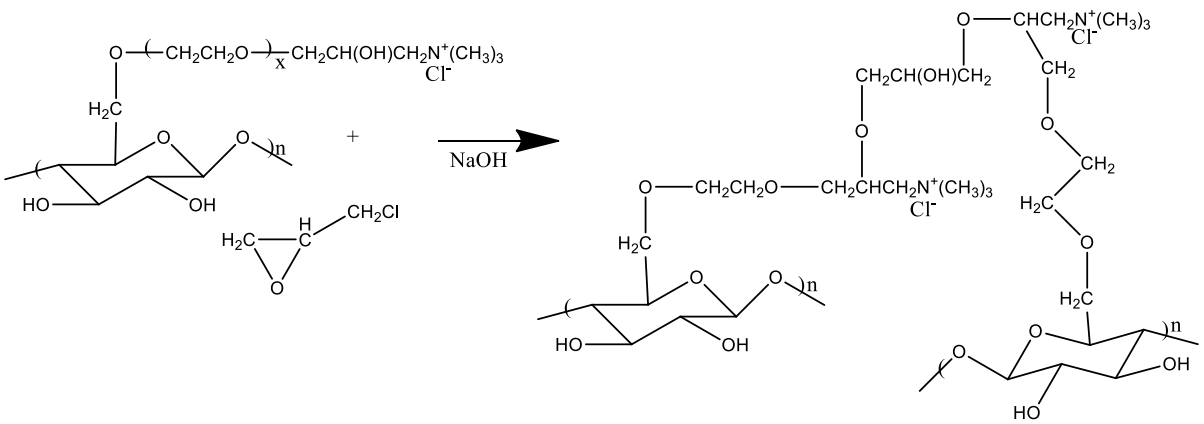

Fig. 2 The cross-linking mechanism of QHEC with E through trimethyl-2-hydroxypropyl group

(unmodified anhydro glycosidic units of HEC, 1 U), 4.94 ppm (1 2-HEC) ppm, and 1 6-HEC at 5.18 ppm hydrogen–deuterium water (D_2O) signal resonated at 4.89 ppm. The ratios of integrated groups were at U/2-HEC/6-HEC = 16.24/4.57/1 (Fig. S2 in SI) and the U/HEC = 2.92 (DS_{2HEC} = 0.21 and DS_{6HEC} = 0.05 and MS = 0.26). The typical anomeric resonances originated from unsubstituted cellulose (1 U, 4.49/104.98 ppm) and HEC substituted 1 H/C unit at 4.55/104.98 ppm as detected in the heteronuclear single quantum coherence (HSQC) spectrum of HEC at 40 °C (Fig. 3). According to correlation spectroscopy (COSY) spectrum the signal of H-1 in the HEC units (4.55 ppm, H-1) is in correlation with H-2 HEC (3.11 ppm) as seen in 2D COSY (Fig. S3 in SI). 2D HSQC enabled the assignment of C-2 in the U unit (85.36 ppm) spectrum due to linkage with H-2; assignment of C-3 (85.94 ppm) was based on combination of 2D HSQC and total correlation spectroscopy (TOCSY) to confirm the H-3 resonated at 3.49 ppm (Fig. S5 in SI). According to COSY, the H-1 of 2-HEC was at 4.50 ppm, which correlates with H-2 of 2-HEC at 3.19 ppm. The C-2 signal was located at 85.07 ppm in the HSQC spectrum of HEC (Fig. 3). The correlation between H-3 in the U unit (3.49 ppm) and H-4 (3.77 ppm); H-2 in HEC (3.12 ppm) and H-4 (3.68 ppm); H-1 in HEC (4.50 ppm) and H-3 (3.69 ppm); H-3 (3.49 ppm) in the unsubstituted cellulose (U) unit and H-4 (3.77 ppm) was done based on the 2D TOCSY spectrum of HEC (Fig. S4 in SI). The signals of C-6 in the $–CH_2–$ group in the U unit were at 3.99, 3.81/62.67 ppm and C-6 in HEC resonated at 3.79, 3.79/72.91 ppm (Table S1 in SI). 2D heteronuclear multiple bond correlation (HMBC; Fig. S6 in SI) confirmed the linkage within the $–CH_2–CH_2–$ (3.52, 72.27, resp. 3.49, 72.77 ppm) array of atoms. These signals were of low intensity in the HSQC spectrum, close to that of 6U at 3.79, 72.91 ppm. ^{13}C spectrum (Fig. S7 in SI) enabled the assignment of carbon signals in all substituted HEC

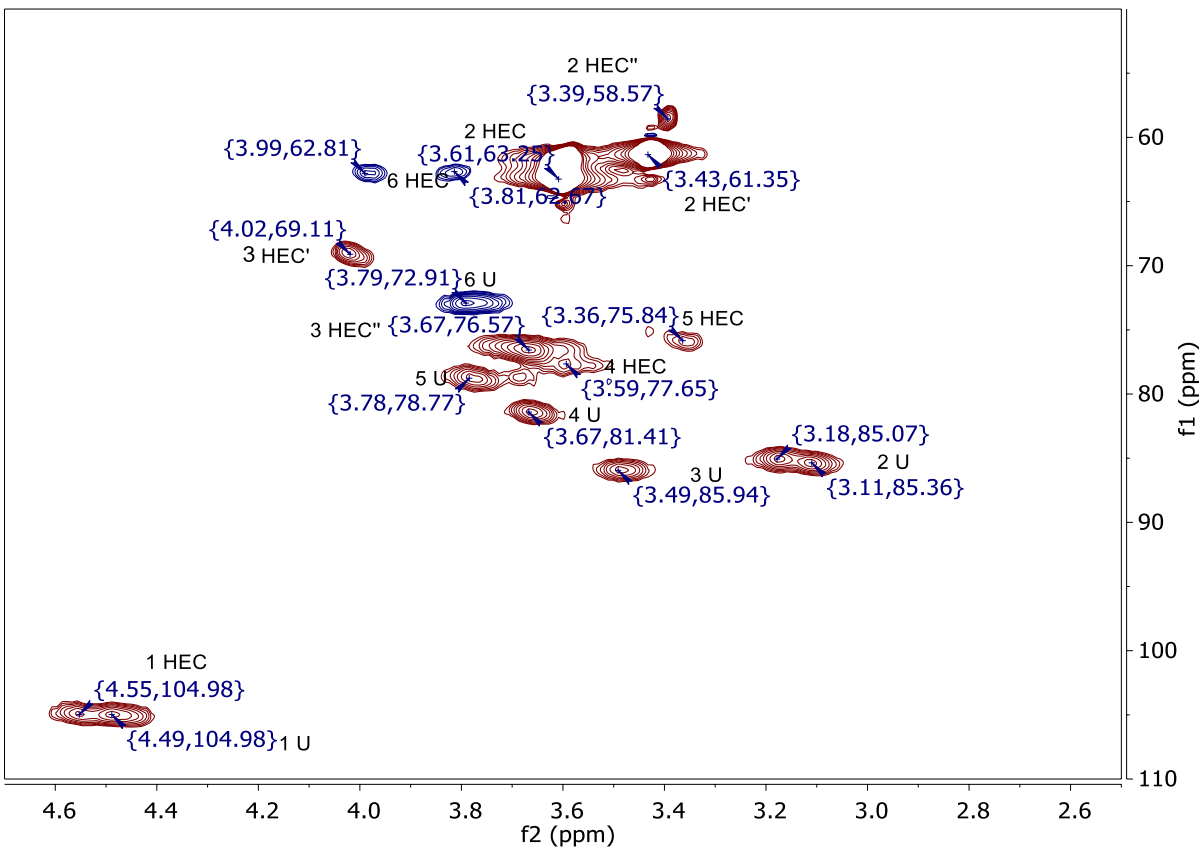

Fig. 3 HSQC spectrum of HEC

groups. The shifts of single- and double-substituted groups at C_2 (R-*CH*–O–CH_2CH_2–O–CH_2–CH_2–OH) and C_3 at 3.67/76.57 ppm and 3.79/72.91 ppm in deuterated dimethylsulphoxide (DMSO-d_6) were also observed before (Li et al. 2014). The multiple substitution on C_3 in DMSO-d_6 was also previously observed (Zhou et al. 2005).

^{1}H-NMR spectrum of CHEC (see the hypothetical structure in Fig. S1) in D_2O (Fig. S8 in SI) was acquired at 15 °C; the anomeric signal shifts of U (4.55 ppm), HEC (4.93 ppm), and CHEC (4.73 ppm) were integrated at the ratio U/HEC/CHEC = 2.52/1/0.04 (DS_C = 0.01, DS_{HEC} = 0.28 and MS_{C+HEC} = 0.29). The anomeric signals of U and HEC in the HSQC spectrum of CHEC were overlapped at 4.53/104.73 ppm. However, they can be distinguished on HSQC-TOCSY spectrum (Fig. S11 in SI) at 4.56/104.46 ppm (H-1/C-1 in U) and 4.48/104.81 ppm (H-1/C-1 in HEC), with CHEC anomeric signal at 4.74/103.75 ppm. The mentioned anomeric signal resolved in HSQC spectrum of CHEC resonated at 4.71/103.72 ppm is related to CHEC (Fig. 4; Table S1 in SI). New –CH_2–CH(OH)–CH_2– bridges could be recognized from the HSQC experiment. The two signals for –CH(OH)– groups at 3.67/82.10 and 3.83/78.77 ppm, were assigned to the 2-hydroxypropyl cross-linking bridges. There are many more new –CH_2– groups, namely at 4.19/74.22, 4.11/74.32, 4.11/65.38, 3.97/74.65, 3.64/74.57, and 3.57/74.73 ppm, indicating both the ethyl substituent and 2-hydroxypropyls cross-linker. The signals of HEC and unsubstituted unit have overlapped chemical shifts as could be seen from Table S1. However, there are more overlapping signals than those observed on HEC. For example, HMBC spectrum of CHEC showed, there are new signals related to 2-hydroxypropyl cross-linker compared to HEC sample. All the related spectra for CHEC are listed in SI (Figs. S9–S13).

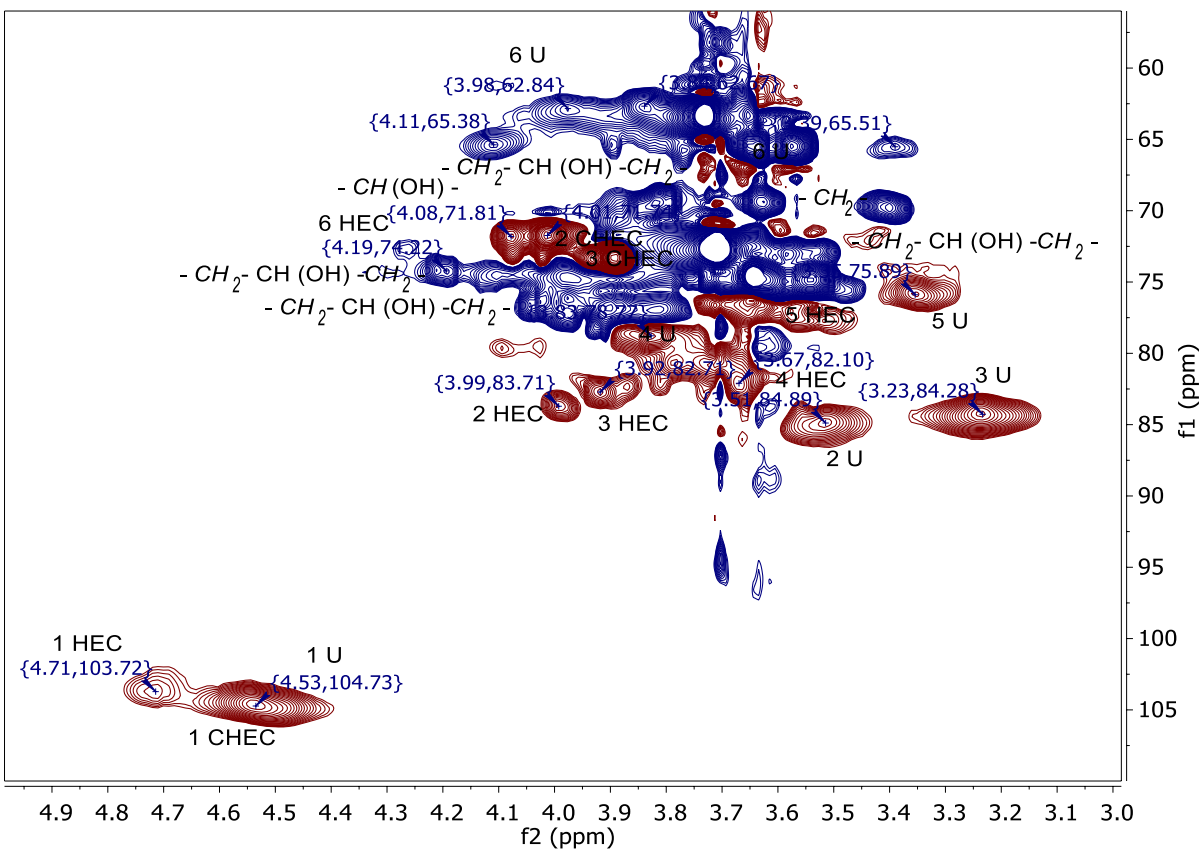

Fig. 4 HSQC spectrum of CHEC

A new signal at 4.43 ppm was observed in the ^{1}H-NMR spectrum of QHEC (Figs. S1, S14 in SI). This is not an anomeric signal, but originates from the –CH(OH)– group of quaternizing substituent. This signal is located next to the H-1 anomeric signal in U (4.56 ppm), H-1 in the QHEC (4.74 ppm), and H-1 in HEC (4.94 ppm). The ratio of signals U/HEC/QHEC = 1.40/0.27/0.27 (DS_Q = 0.14 and MS_{Q+HEC} = 0.10). The HSQC spectrum of QHEC (Fig. 5) showed the anomeric signals of U and QHEC were overlapped at 4.56/104.82 and 4.54/104.98 ppm. The remaining anomeric signal of HEC substituents was observed at 4.75/103.94 ppm. Based on COSY spectrum of QHEC (Fig. S15) the correlation between the substituent –CH(OH)– group (4.43, 67.79 ppm) and –CH_2– groups was located at 3.67/74.52 ppm and 3.68/63.34 ppm, respectively. Signals at 3.84/76.84, 3.67/74.52, 3.93/74.67 and 4.01/74.67 ppm correspond to the quaternized group, while the three methyl groups linked to the introduced ammonium nitrogen is at 3.25/56.95 ppm and could not take part in correlation due to five-bond distance. Based on HSQC-TOCSY analysis (Fig. S16 in SI), we assume the anomeric signal of unsubstituted cellulose (4.56/104.58 ppm) is the strongest one (Table S1 in SI). The intensity of quaternized spacer signals in QHEC was weaker than that observed in CHEC substitution.

According to ^{1}H-NMR of QCHEC (Fig. S1) sample (Fig. S19 in SI), the QCHEC, QHEC, and CHEC anomeric signals are overlapping at 4.75 ppm. The ratio of U/HEC/QCHEC + QHEC + CHEC = 1.99/0.50/1.00 (DS_{QC} = 0.29, DS_{HEC} = 0.14 and MS_{QC+HEC} = 0.43). (DS_{QC} MS_{QC+HE}). Only two anomeric signals were observed in the HSQC spectrum of QCHEC sample (Fig. 6); the predicted structure is shown in Fig. S1, SI. Stronger anomeric signal at 4.56/104.73 ppm originates from the unmodified cellulose, and is overlapped with HEC, CHEC, QHEC, and QCHEC at 4.74/104.12 ppm. The positions of

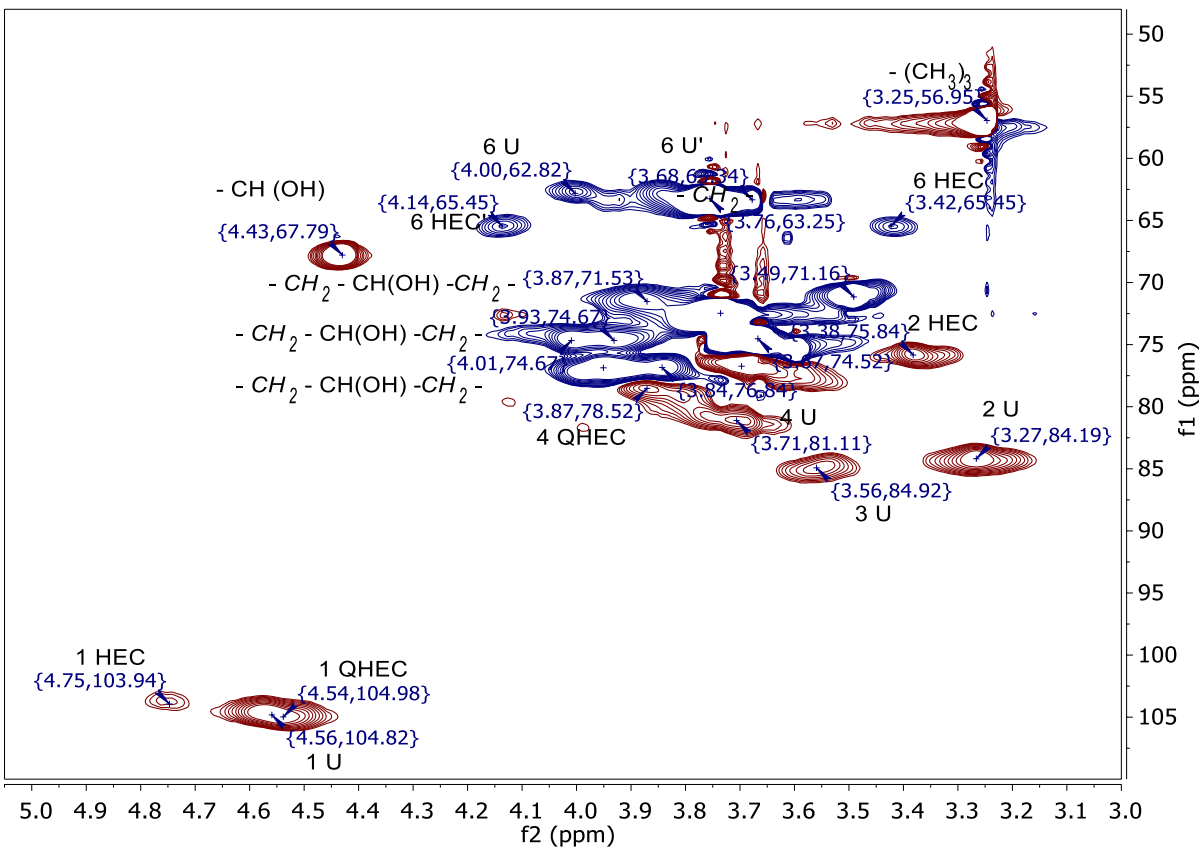

Fig. 5 HSQC spectrum of QHEC

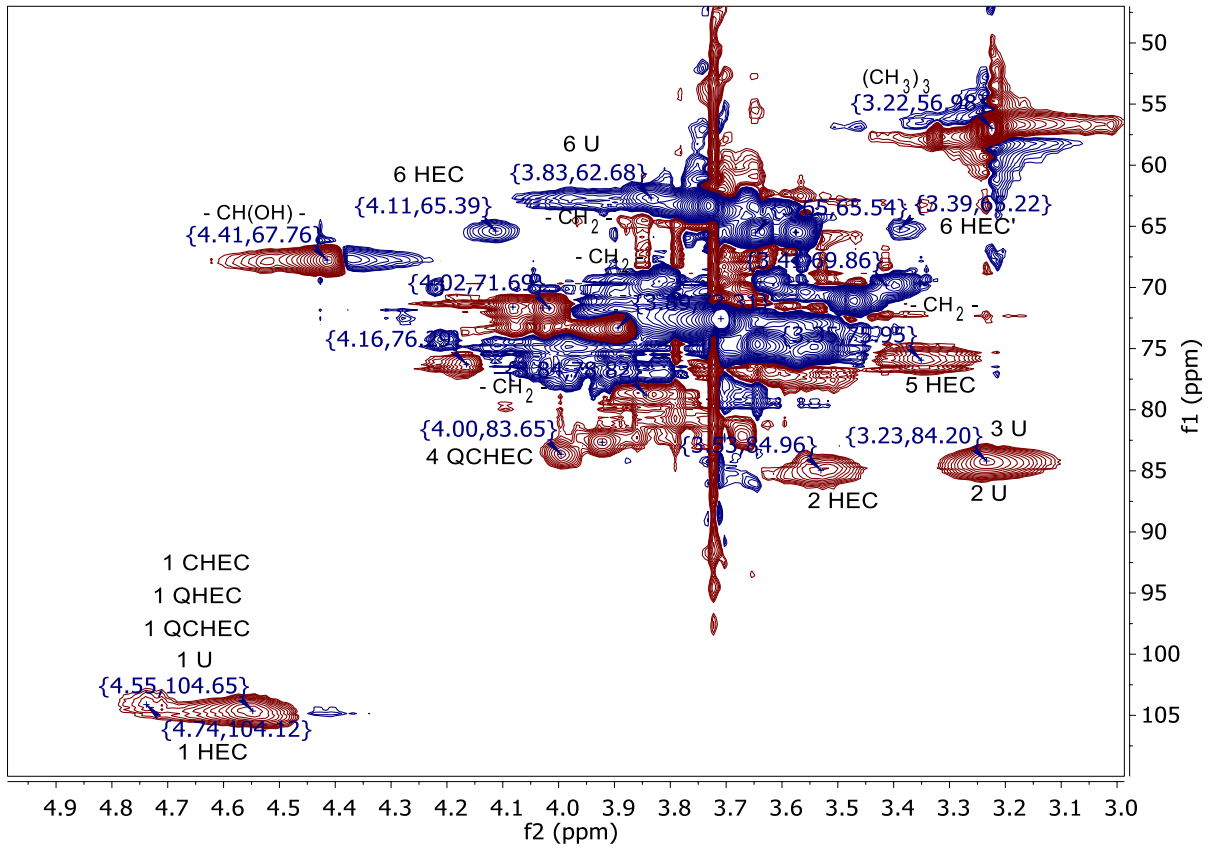

Fig. 6 HSQC spectrum of QCHEC

individual signals are similar to previous samples and are listed in SI in Table S1. The significant $(CH_3)_3$ signal linked to quaternary nitrogen was located at 3.22/56.98 ppm. The three most intense signals at 4.43/67.70, 4.03/71.68 and 3.91/73.34 ppm are related to –CH(OH) signals of the $–CH_2–CH(OH)–CH_2–$ and $–CH_2–CH(OH)–CH_2–N^+(CH_3)_3$ spacers, respectively. According to HSQC-TOCSY and HMBC spectra of QCHEC (Figs. S22 and S23 in SI) the remaining signals correlate with spectra of CHEC and QHEC samples. The three different CH_2OH signals could be distinguished with the aid of HMBC spectrum of QCHEC and the chemical shifts listed in Table S1 in SI. It seems that the quaternary spacer is linked to HEC substituent and through the cross-linking agent. This resulted in a number of overlapping signals of $-CH_2-$ and -CH(OH)- groups. The NMR data of all four derivatives are summarized in the Table S1 in SI.

SEC-MALS analysis

The Fig. 7 shows the conformation plots of $R_g = f(M)$ of HEC, QCHEC, QHEC, and QCHEC in carbonate buffer at pH 10. Radius of gyration represents the size of formed macromolecule coils; following R_g values were obtained: QHEC (38–260 nm) > QCHEC (10–230 nm) > CHEC (21–100 nm) > HEC (23–50 nm). The cross-linking of HEC (CHEC sample) led to appearance of a second peak in conformation plot which corresponded to formation of a higher molecular weight. Quaternization caused the decrease of molecular weight at the peak (M_p), as seen for QHEC and QCHEC shifting to lower values with respect to that of HEC. Compared to HEC sample, the R_g values of CHEC were only measurable at higher molecular weights ($> 6 \times 10^6$ g/mol) and were less scattered. The R_g values for QHEC and QCHEC showed signs of increasing trend for higher molecular weights, however the measured values were

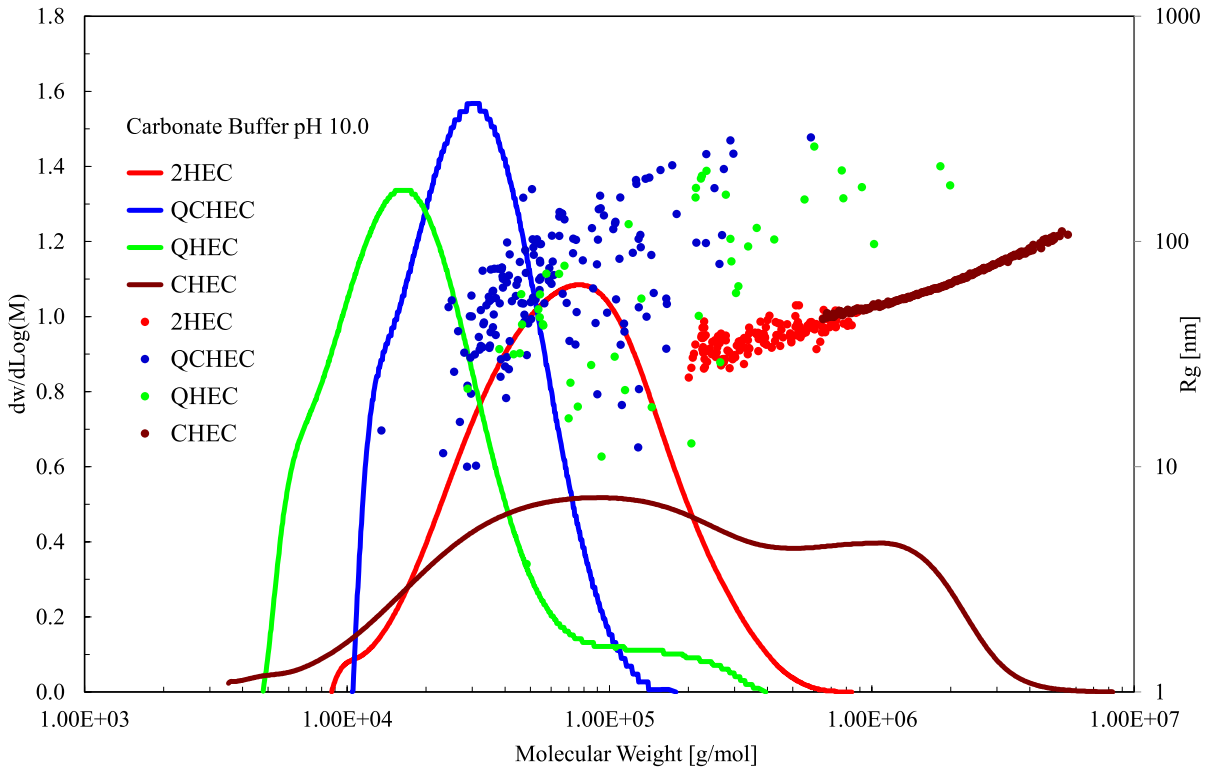

Fig. 7 Conformation plots and $R_g = f(M)$ of HEC (red), CHEC (brown), QHEC (green), and QCHEC (blue) measured in water-carbonate buffer at pH 10

distributed across much wider range. This could be explained by the repulsive forces among the quaternary groups which resulted in larger macromolecule coil volumes. Additionally, water solubility of the individual samples may also play a role; following solubilities were determined: HEC (98%) > CHEC (72%) > QHEC (26%) > QCHEC (14%). The composition of the films was as follows. The HEC film contained 98% water-soluble part and 2% was assumeed to be insoluble residual crystalline CII. The CHEC film contained 72% soluble part which according to NMR was monofunctionally hydroxypropyl-modified HEC, then 26% was bi-functionally crosslinked hydroxypropyl-O-hydroxyethylcellulose, and the rest 2% was residual chemically unmodified crystalline cellulose (CII). The QHEC film consisted of 26% of water-soluble quaternized cellulose, 72% of insoluble multiple-quaternized-O-hydroxyethylated cellulose, and the rest 2% was residual crystalline CII. The QCHEC consisted of 14% of water-soluble quaternized and mono-functionally-substituted 2-hydroxypropyl-O-hydroxyethyl cellulose, then the 84% was bi-functionally substituted, insoluble 2-hydroxyepropyltrimetylammonium-hydroxypropyl-O-hydroxyethyl cellulose, and the rest 2% was residual crystalline CII. All this was confirmed from the SEC-MALS analysis, NMR, and FTIR spectroscopy. The soluble and insoluble components are just differeing in mono and multiple bonding through hydroxypropyl-O-hydroxyethyl bridges. Based on the known mechanisms of quaternization and crosslinking and the results of analysis on water-soluble part and films we could assume that there are similarities in structures between the soluble and insoluble products of the reactions. But according to MS and M_w values the structures of CHEC and QCHEC were not rod-like (Yoshida et al. 2024).

FTIR analysis of films

Due to the decreased solubility of CHEC, QHEC, and QCHEC samples compared to HEC, prepared

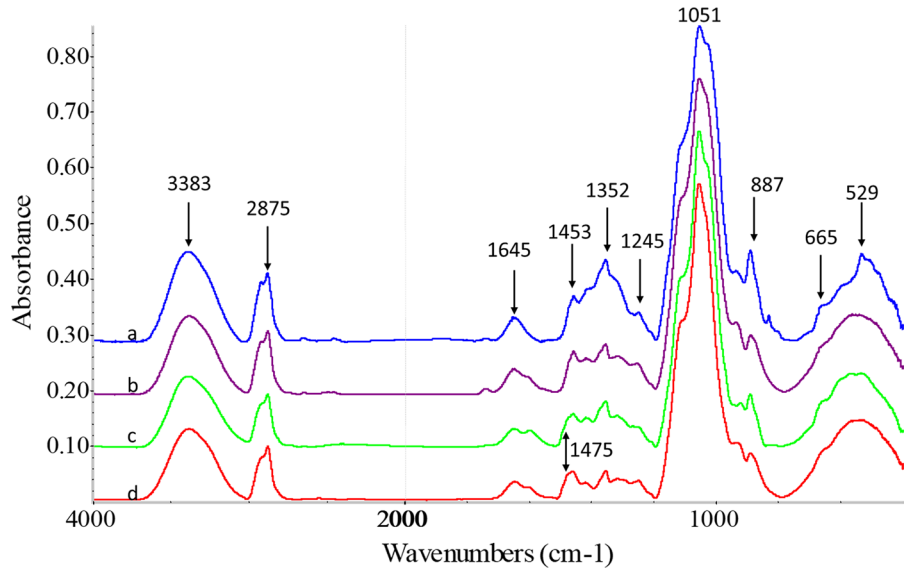

Fig. 8 FTIR spectra of prepared films: **a** HEC, **b** CHEC, **c** QHEC, and **d** QCHEC

films were investigated by Fourier-transform infrared spectroscopy. The acquired spectra (Fig. 8) showed broad absorption peaks at 3383 cm^{-1} representing the stretching vibrations of hydroxy groups. The bands observed at 2917 cm^{-1} and 2875 cm^{-1} are related to C-H stretching vibrations in CH_2 and CH_3 groups. Although the above-mentioned bands are present in most of the polysaccharides, their breadth in HEC varies with its molar weight and crystallinity (Şen and Kahraman 2018). The 1500–1200 cm^{-1} region revealed peaks which corresponded to CH_2 (1417 cm^{-1}) and C–H vibrations (1352 cm^{-1}) and to C–O–H bending vibrations at all unsubstituted positions. Comparable results for C-H vibrations (1352–1353 cm^{-1}) were recorded for solid HEC electrolyte prepared by solution casting on glass petri dishes. The strongest absorption peaks were observed at 1100–900 cm^{-1} region. This region is known to be related to HEC ether bonds (1160 and 926 cm^{-1}; Masry et al. 2024). Further observed were the bands representing asymmetric C–O–C vibrations located at 1113 cm^{-1}, C–O anti-symmetric vibrations in anhydroglucose units of hydroxyethyl cellulose at 1051 cm^{-1}, and the absorption band of C–C stretching vibrations in the glucopyranose structure at 1021 cm^{-1} (Bajaber et al. 2022). The band at 887 cm^{-1} corresponds to the β–(1 → 4)-glycosidic linkages backbone. The most important new C–N stretching vibration of QHEC (Fig. 8c) and QCHEC (Fig. 8d) is seen as a shoulder at 1475 cm^{-1} linked to the quaternary group was also confirmed (Şen and Kahraman 2018). The region between 1700 and 1200 cm^{-1} has similarities for CHEC, QHEC, and QCHEC samples. This could be explained by the presence of 2-hydroxypropyle group in both quaternary spacer and cross-linking bridge. The data acquired using the KBr technique at 1460 and 933 cm^{-1} gave negligible response (Wang and Ye 2010).

TG/DTG/DTA analysis

Onset temperatures for HEC derivatives were evaluated from the TG/DTG/DTA analysis (Table S3 in SI); following values were determined: HEC (222 °C) > QCHEC (162 °C) > CHEC (142 °C) > QHEC (141 °C). The QHEC and CHEC samples were found to have only 11% residue left at 500 °C. It indicates similar thermal stability of quaternary ammonium group and 2-hydroxyethyl bridge formed by epichlorohydrin crosslinking. Trimethylammonium group degrades in inert environment into trimethylamine, 3-hydroxy-2-propane,

and water (Šimkovic et al. 1985a). The thermooxidative effect of trimethylammonium-2-hydroxypropyl-quaternary group is similar to that of unmodified cellulose (Šimkovic et al. 1985b) and to that of HEC. Our results confirm, that the prepared film samples are more thermally stable compared to the case when they are in powder form. This behaviour results from their much smaller surface area in film from.

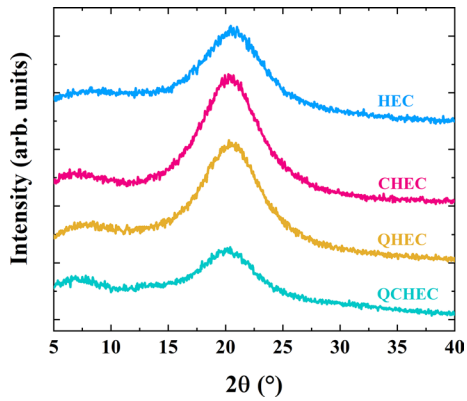

Fig. 9 Symmetric XRD scans of HEC, CHEC, QHEC, and QCHEC films (top to bottom)

XRD analysis

Crystallinity of prepared HEC, CHEC, QHEC, and QCHEC film samples was investigated by symmetric XRD scanning (Fig. 9); no significant differences were observed among the samples. Only a residual crystallinity in all four samples was confirmed by the single significant feature observed at 2θ = 20–21° and a weak signal found at ~ 7° related to HEC (French 2014). Our results did not confirm other previously reported CII-related XRD peaks typical for HEC prepared under alkaline conditions, i.e. those at ~ 12° and 21.8° (Taghizadeh and Seifi-Aghjekohal 2015, Li et al. 2014) suggesting lower degree of ordering of HEC-based films studied here. The absence of peaks at ~ 14.8, 16.3, and 22.6° which are typical for raw cellulose indicates negligible concentration of cellulose I (CI) in prepared HEC-based films (Li et al. 2014). We conclude that the used chemical modification of HEC under alkaline conditions did not significantly alter the crystallinity in produced HEC derivatives compared to base HEC and no new crystalline (e.g., cellulose-related) components were formed. Assuming the SEC-MALS-determined water-solubility of HEC (98%), the content of crystalline component was only 2%. Similar crystalline content can be expected for all derivatives, because only the hydroxy groups are modified by quaternization with GTMAC or cross-linking with E. This is

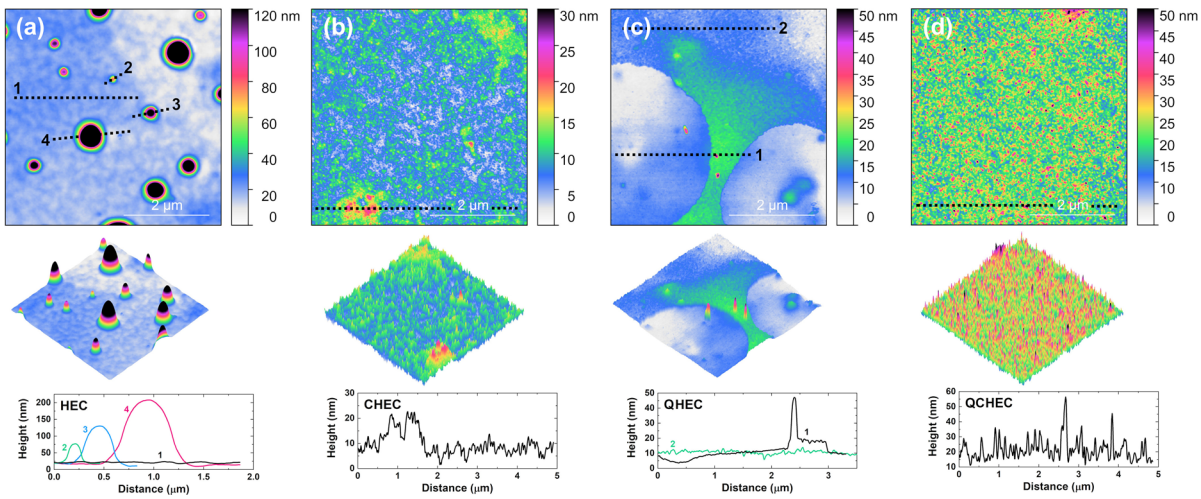

Fig. 10 AFM-resolved surface morphology of **a** HEC, **b** CHEC, **c** QHEC, and **d** QCHEC films

because the native cellulose hydroxy groups cannot be attacked by the alkylating agents and every new hydroxyl group formed on cross-linker or alkylating agent can further react with the epoxy ring on E or GTMAC (Šimkovic et al. 2020). The above data could be further supported by additional references, which excluded the presence of CII (French 2020a, b; Yao et al. 2020).

AFM analysis

Selected representative line profiles were taken along dashed lines.

AFM was used to study the surface morphology of all four HEC-based film samples; significant differences were found (Fig. 10). The HEC substrate showed very smooth surface with frequent occurrence (~ 3.7×10^7 cm^{-2}) of spherical particles of various sizes. The determined root-mean-square (RMS) surface roughness was 25 nm when the particles were included, or 1.6 nm when they were excluded. Two main size ranges of particles were observed, i.e. (i) the most frequent: diameter (d) ~ 240 nm, height (h) ~ 120 nm and (ii) less frequent: d ~ 700–1100 nm, h ~ 70 nm and ~ 220–400 nm. CHEC and QCHEC films showed granular surface with RMS surface roughness of 2.8 nm and 5.8 nm, respectively. Surface of QHEC film was also somewhat granular, however, it contained circular depressions/holes d ~ 4 µm. The bottom of the depressions was smooth and free of the granular structure present elsewhere on the QHEC film. RMS surface roughness of QHEC film was 4.2 nm.

We believe the observed spherical particles likely consisted of unmodified cellulose, insoluble part and/or supramolecular aggregates resulting from intermolecular hydrophobic association as described elsewhere (Bai et al. 2018).

To compare the grain sizes in CHEC, QHEC, and QCHEC films, a first order approximation using height autocorrelation was used. 1D autocorrelation function (1D-ACF) was calculated for all three films in Gwyddion software and Gaussian fit was used to find the average grain size (Nečas et al. 2012). Following 1D-ACF-determined grain sizes were found: QCHEC (~ 34 nm) < CHEC (~ 55 nm) < QHEC (~ 59 nm). While CHEC and QHEC grain sizes were comparable and within the accuracy of the used evaluation method, QCHEC showed significantly smaller grain size. This smaller grain size may be reflecting the increased cross-linking density in the QCHEC sample, related to the presence of additional hydroxy groups at 2-hydroxypropylammonium position of the quaternary group.

Conclusions

In conclusion, we prepared HEC derivatives under alkali conditions by quaternization with GTMAC, cross-linking with E, and by a combination of both. Quaternized and cross-linked derivative was prepared by one-step method. Structural, physical, and chemical properties of produced liquid and film samples were comprehensively studied by NMR, SEC-MALS, FTIR, TG/DTG/DTA, XRD, and AFM. To evaluate the potential improvement of prepared HEC-based derivatives, we used combination of analytical methods and bring new valuable insights into the structure and properties of prepared HEC derivatives. In particular, by using the combination of NMR method in D_2O solution of HEC derivatives and FTIR measurement on HEC and HEC-based films, we can conclude that the solution and film compositions were identical. Following water-solubility was found by SEC-MALS: HEC (98%) > CHEC (72%) > QHEC (26%) > QCHEC (14%). According to obtained R_g values, it was found, that the components of films were forming coil structures within the range below and up to 100 nm (HEC and CHEC) or in the range ~ 10–300 nm (QHEC and QCHEC). We concluded, that their formation was likely caused by the repulsive quaternary ammonium groups. Different broad band signals for –OH and $–CH_2–$ groups were confirmed by FTIR in HEC derivatives, which we ascribed to the difference in their supramolecular structures. These differences were expressed by the bands at 3383 cm^{-1} for -OH and 2875 cm^{-1} for $–CH_2–$ groups of HEC. TG/DTG/DTA analysis showed various OTs for prepared HEC-based derivatives: HEC (222 °C) > QCHEC (162 °C) > CHEC (142 °C) > QHEC (141 °C. XRD showed low degree of ordering of HEC-based derivatives without

notable differences among all four studied films; only residual crystallinity related to CII was confirmed. Presence of CI was excluded. Therefore, we conclude the used chemical modifications of HEC under alkaline conditions did not cause any significant crystallinity change in produced derivatives and no new crystalline components were formed. AFM showed significant differences in surface morphology among the studied HEC-based films. While HEC film showed smooth surface with large and frequent spherical particles, CHEC, QHEC, and QHEC films exhibited granular surface. Moreover, QHEC film contained circular depressions/holes with diameter ~ 4 µm. Following RMS surface roughness values were found: CHEC (2.8 nm) < QHEC (4.2 nm) < QCHEC (5.8 nm) < HEC (25 nm). 1D-AFC analysis estimated following grain sizes: QCHEC (~ 34 nm) < CHEC (~ 55 nm) < QHEC (~ 59 nm). Significantly larger grain size in QCHEC might be reflecting better opportunities for cross-linking through the 2-hydroxypropyl(trimethylammonium) group. Prepared HEC-based composite films represent bio-degradable polysaccharide materials, potentially important for a large number of applications including, environmentally-friendly packaging and protective coating which can help to lower the use of synthetic plastics in some of the medical and food application and reduce the amount of long-term stable waste, harmful to various ecosystems. Also, some of the prepared derivatives can find their purpose in various industries such as, in construction technology or textile production, where they can help to reduce the use of some of the typically-used harmful chemicals.

Acknowledgments Hana Kováčová is acknowledged for running the elemental analysis, and Zuzana Netriová for the TG/DTG/DTA analysis.

Author contributions Author contributions to the present study according to CRediT taxonomy are as follows. Conceptualization: I.Š., F.G., M.H. (Miloš Hricovíni). Formal analysis: M.H. (Michal Hricovíni), F.G., E.D., Funding acquisition: M.H. (Miloš Hricovíni). Investigation: I.Š., F.G., M.H. (Michal Hricovíni), R.M., E.D, V.D., J.F.. Methodology: I.Š., F.G., M.H. (Miloš Hricovíni), R.M. Project administration: I.Š., M.H. (Miloš Hricovíni). Supervision: I.Š. Validation: I.Š., F.G., R.M., M.H. (Miloš Hricovíni). Visualization: I.Š., F.G. Writing – original draft: I.Š. Writing – review and editing draft: I.Š., F.G., M.H., V.D., J.F., M.H. (Miloš Hricovíni), R.M., E.D., A.G.S., D.P., S.Z, J.F.

Funding Open access funding provided by The Ministry of Education, Science, Research and Sport of the Slovak Republic in cooperation with Centre for Scientific and Technical Information of the Slovak Republic. This article was funded by Vedecká Grantová Agentúra MŠVVaŠ SR a SAV, 2/0071/22.

Data availability No datasets were generated or analysed during the current study.

Declarations

Conflict of interest The authors declare that they have no conflict of interest.

Ethical approvals Not applicable.

References

Bai Y, Shang X, Wang Z, Zhao X (2018) Experimental study on hydrophobically associating hydroxyethyl cellulose flooding system for enhanced oil recovery. Energy & Fuels 32(6):6713–6725. https://doi.org/10.1021/acs.energyfuels.8b01138

Bajaber MA, Anjum MN, Ibrahim M, Farooq T, Ahmad MN, Abideen Z (2022) Synthesis and characterization of hydroxyethyl cellulose grafted with copolymer of polyaniline and polypyrrole biocomposite for adsorption of dyes. Molecules 27(23):8238. https://doi.org/10.3390/molecules27238238

Busk A, Van Der Horst PM, Holger P, Yonghua T (2004) Use of a quaternary ammonium alkyl hydroxethyl cellulose ether as a conditioner for hair and skin. US 2004/0151681 A1.

Cho J, Waetzig GR, Udayakantha M, Hong CY, Banerjee S (2018) Incorporation of hydroxyethylcellulose-functionalized halloysite as a means of decreasing the thermal conductivity of oilwell cement. Sci Rep 8:16149. https://doi.org/10.1038/s41598-018-34283-0

Chu HY, Hong JY, Huang CF, Wu JY, Wang TL, Wu TM, Lee RH (2019) Enhanced photovoltaic properties of perovskite solar cells by the addition of cellulose derivatives to MAPbI3 based photoactive layer.

Cellulose 26:9229–9239. https://doi.org/10.1007/s10570-019-02724-2
Cofer KB (1958) Continuous hydrolysis of epichlorohydrin. US 2838574A.
Del Giudice F, Tassieri M, Oelschlager C, Shen AQ (2017) When microrheology, bulk rheology, and microfluids meet: broadband rheology of hydroxyethyl cellulose water solutions. Macromolecules 50:2951–2963. https://doi.org/10.1021/acs.macromol.6b02727
Diao Y, Song M, Zhang Y, Shi L, Lv Y, Ran R (2017) Enzymatic degradation of hydroxyethyl cellulose and analysis of the substitution pattern along the polysaccharide chain. Carbohydr Polym 169:92–100
French AD (2014) Idealized powder diffraction patterns for cellulose polymorphs. Cellulose 21:885–896. https://doi.org/10.1007/s10570/013/0030-4
French AD (2020a) Increment in evaluation of cellulose crystallinity analysis. Cellulose 27:5445–5668. https://doi.org/10.1007/s10570-020-031172-z
French AD (2020b) Increment in evaluation of cellulose crystallinity analysis. Cellulose 27:9135–9136. https://doi.org/10.1007/s10570-020-03377-2
Gökmen FÖ, Bayramgil NP (2022) Preparation and characterisation of some cellulose derivatives nanocomposite films. Carbohydr Polym 297:120030. https://doi.org/10.1016/j.carbpol.2022.120030
Kim J, Rackstraw NB, Weinstein TJ, Reiner B, Leal L, Ogawa K, Dauenhauser PJ, Reineke TM (2024) Cellulose etherification with glycidol for aqueous rheology modification. ACS Appl Polym Mater 6:6714–6725. https://doi.org/10.1021/acsapm.4c01002
Kuniak L, Marchessault RH (1972) Study of the crosslinking reaction between epichlorohydrin and starch. Starch/starke 24:110–116. https://doi.org/10.1002/star.1972020404
Langan P, Sukumar N, Nishiyama Y, Chanzy H (2005) Synchrotron X-ray structures of cellulose Iβ and regenerated cellulose II at ambient temperature and 100 K. Cellulose 12:551–562. https://doi.org/10.1007/s10570-005-9006-3
Li F, Wang W, Wang X, Yu J (2014) Changes of structure and property of alkali soluble hydroxyethyl celluloses (HECs) and their regenerated films with the molar substitution. Carbohydr Polym 114:206–212. https://doi.org/10.1016/j.carbpol.2014.08.015
Luo C, Ma H, Yu H, Zhang Y, Shao Y, Yin B, Ke K, Zhao L, Zhang K, Yang MB (2023) Enhanced Triboelectric nanogenerator based on a hybrid cellulose aerogel for energy harvesting and self-powered sensing. ACS Sustainable Chem Eng 11:9424–9432. https://doi.org/10.1021/acssuschemeng.3c01369
Masry BA, Gayed HM, Daoud JA (2024) Gamma radiation synthesis of hydroxyethyl cellulose/acrylic acid/CYANEX 471X hydrogel for silver ionic capture from acidic nitrate medium. Cellulose 31:4329–4346. https://doi.org/10.1007/s10570-024-05869
Nečas D, Klapetek P (2012) Gwyddion: an open-source software for SPM data analysis. Cent Eur J Phys 10:181–188
Odabas N, Amer H, Bacher M, Henninges U, Potthast A, Rosenau T (2016) Properties of cellulosic material after cationization in different solvents. ACS Sustain Chem Eng 4:2295–2301. https://doi.org/10.1021/acssuschemeng.5b01752
Olson E, Blisko J, Du C, Liu Y, Li Y, Thurber H, Curtzwiler G, Ren J, Thuo M, Yong X, Jiang S (2021) Biobased superhydrophobic coating enabled by nanoparticle essembly. Nanoscale Adv. 3:4037. https://doi.org/10.1039/dina00296a
Schaubeder JB, Ganser C, Nypelo T, Uchihashi T, Spirk S (2024) How resilient is wood xylan to enzymatic degradation in a matrix with kraft lignin? Biomacromolecules 25:3532–3541. https://doi.org/10.1021/acs.biomac.4c00185
Şen F, Kahraman MV (2018) Preparation and characterization of hybrid cationic hydroxyethyl cellulose/sodium alginate polyelectrolyte antimicrobial films. Polym Adv Technol 29:1895–1901. https://doi.org/10.1002/pat.4298
Šimkovic I (2008) What could be greener than composites made from polysaccharides? Carbohydr Polym 74:759–762. https://doi.org/10.1016/j.carbpol.2008.07.009
Šimkovic I (2013) Unexplored possibilities of all-polysaccharide composites. Carbohydr Polym 95:697–715. https://doi.org/10.1016/j.carbpol.2013.03.040
Šimkovic I, Jakab E (2001) Thermogravimetry/mass spectrometry study of weakly basic starch-based ion exchanger. Carbohydr Polym 45:53–59
Šimkovic I, Antal M, Mihálov V, Königstein J, Micko MM (1985a) Influence of anionic form on thermal degradation of TMAHP-cellulose. J Appl Polym Sci 30:4707–4711
Šimkovic I, Antal M, Balog K, Košík Š, Plaček J (1985b) Influence of anionic form on thermo- oxidation of TMAHP-cellulose. J Appl Polym Sci 30:4713–4721
Šimkovic I, Hricovíni M, Šoltés L, Mendichi R, Cosentino C (2000) Preparation of water-soluble/insoluble derivatives of hyaluronic acid by cross-linking with epichlorohydrin in aqueous NaOH/NH_4OH solution. Carbohydr Polym 41:9–14
Šimkovic I, Hricovíni M, Sasinková V (2002) Preparation of ion-exchangers by cross-linking of starch or polygalacturonic acid with 1, 3-bis (3-chloro-2-hydroxypropyl) imidazolium hydrogen sulfate. Carbohydr Polym 47:131–136
Šimkovic I, Mendichi R, Uhliariková I (2008) Modification of polygalacturonic acid hydroxyls with trimethylammonium- and/or sulfonate-2-hydroxypropyl group. Carbohydr Polym 74:611–616. https://doi.org/10.1016/j.carbpol.2008.04.024
Šimkovic I, Yadav MP, Zalibera M, Hicks KB (2009a) Chemical modification of corn fiber with ion-exchanging groups. Carbohydr Polym 76:250–254. https://doi.org/10.1016/j.carbpol.2008.07.009
Šimkovic I, Synytsya A, Uhliariková I (2009b) Čopíková J (2009b) Amidated pectin derivatives with n-propyl-, 3-aminopropyl-, 3-propanol or 7-aminoheptyl-substituents. Carbohydr Polym 76:602–606. https://doi.org/10.1016/j.carbpol.2008.11.022
Šimkovic I, Uhliariková I, Yadav MP, Mendichi R (2010) Branched arabinan obtained from sugar beet pulp by quaternization under acidic conditions. Carbohydr Polym 82:815–821. https://doi.org/10.1016/j.carbpol.2010.05.057
Šimkovic I, Šurina I, Mikulášik R, Orságová A, Ház A, Schwarzinger C (2013) Evaluation of the phytomass

source for composite preparation. J Appl Polym Sci 127:508–515. https://doi.org/10.1002/app.37807

Šimkovic I, Tracz A, Kelnar I, Uhliariková I, Mendichi R (2014a) Quaternized and sulfated xylan derivative films. Carbohydr Polym 99:356–364. https://doi.org/10.1016/j.carbpol.2013.08.075

Šimkovic I, Kelnar I, Uhliariková I, Mendichi R, Mandalika A, Elder T (2014b) Carboxymethylated-, hydrxypropylsulfonated- and quaternized xylan derivative films. Carbohydr Polym 110:464–471. https://doi.org/10.1016/j.carbpol.2014.04.055

Šimkovic I, Mendichi R, Kelnar I, Filip J, Hricovíni M (2015) Cationization of heparin for film applications. Carbohydr Polym 115:551–558. https://doi.org/10.1016/j.carbpol.2014.09.021

Šimkovic I, Kelnár I, Mendichi R, Bertók T, Filip J (2017) Composite films prepared from agricultural by-products. Carbohydr Polym 156:77–85. https://doi.org/10.1016/j.carbpol.2016.09.014

Šimkovic I, Gucmann F, Mendichi R, Giacometti Schieroni A, Piovani D, Dobročka E, Hricovíni M (2021) Extraction and characterization of polysaccharide films from *Furcellaria lumbricalis* and *Gigartina skottsbergii* seaweeds. Cellulose 28:9567–9588. https://doi.org/10.1007/s10570-021-04138-5

Šimkovic I, Gucmann F, Hricovíni M, Mendichi R, Giacometti Schieroni A, Piovani D, Zappia S, Dobročka E, Filip J, Hricovíni M (2023) Properties of quaternized and crosslinked carboxymethilcellulose films. Cellulose 30:2023–2036. https://doi.org/10.1007/s10570-022-05031-5

Solhi L, Guccini V, Heise K, Solala I, Niinavaara E, Xu W, Mihhels K, Kröger M, Meng Y, Wohlert J, Tao H, Cranston ED, Kontturi E (2023) Understanding nanocellulose-water interaction: turning a determinant into asset. Chem Rev 123:1925–2015. https://doi.org/10.1021/acs.chemrev.2c00611

Stoyneva V, Momekova D, Kostova B, Petrov P (2014) Stimuli sensitive super-macroporous cryo gel based on photo-crosslinked 2-hydroxyethylcellulose and chitin. Carbohydr Polym 99:825–830. https://doi.org/10.1016/j.carbpol.2013.08.095

Taghizadeh MT, Seifi-Aghjekohal P (2015) Sonocatalytic degradation of 2-hydroxyethyl cellulose in the presence of some nanoparticles. Ultras Sonochem 26:265–272

Wang K, Ye L (2010) Structure and property of cationic hydroxyethyl cellulose. Polym-Plast Technol Eng 49:807–811. https://doi.org/10.1080/036025510003749619

Xu F, Cho B-U (2024) Porous cationic cellulose beads prepared by homogeneous in-situ quaterni-zation and acid induced regeneration for water/moisture absorption. Carbohydr Polym 340:122301. https://doi.org/10.1016/j.carbpol.2024.122301

Yao W, Weng Y, Catchmark JM (2020) Improved cellulose X-ray diffraction analysis using Fourier series modelling. Cellulose 27:5563–5579. https://doi.org/10.1007/s10570-020-03177-8

Yoshida M, Iwase H, Horikawa Y, Shikada T (2024) Evidence of a rod-like structure for hydroxy-propyl cellulose samples in aqueous solution. Biomacromolecules 25:4255–4266

Zhou Q, Zhang L, Li M, Wu X, Cheng G (2005) Homogeneous hydroxyethylation of cellulose in NaOH/urea aqueous solution. Polym Bull 53:243–248. https://doi.org/10.1007/s00289-005-0334-0